Supporting Online Material for

Detection, Stimulation, and Inhibition of Neuronal Signals with High-Density Nanowire Transistor Arrays

Fernando Patolsky, Brian P. Timko, Guihua Yu, Ying Fang, Andrew B. Greytak, Gengfeng Zheng, Charles M. Lieber*

*To whom correspondence should be addressed. E-mail: cml@cmliris.harvard.edu

Published 25 August, *Science* **313**, 1100 (2006)
DOI: 10.1126/science.1128640

This PDF file includes:

Materials and Methods

Nanowire (NW) array fabrication. The 20 nm diameter silicon NWs (SiNWs) were synthesized by gold nanocluster chemical vapor deposition as described previously *(1-3)*. Diborane and phosphine with B:Si and P:Si ratios of 1:4000 were used to prepare p-type and n-type NWs, respectively. NWs were aligned on oxidized surface of silicon chips (600 nm thick oxide, NOVA Electronic Materials, Ltd.) using flow-directed *(4)* or Langmuir-Blodgett *(5)* techniques, where a uniform parallel NW array with controlled separation could be prepared over entire chip with the latter method. Source and drain contacts to the NWs were defined following assembly using reported photolithography and metal deposition (60 nm Ni), and were passivated prior to resist lift-off by deposition of ca. 150 nm thick Si_3N_4 by plasma-enhanced CVD. A multilayer photoresesist structure consisting of 300 nm LOR3A (Microchem) and 500 nm 1805 (Shipley) was typically exposed with 365 nm light for 0.8 s (24 mW/cm^2) using an AB-M mask aligner (manufacturer), and then developed in CD-26 developer to undercut the LOR3A ca. 250 nm. The undercut enables complete passivation of metal electrodes during the Si_3N_4 deposition in a single photolithography step.

Chip surface patterning. A second photolithography step was used to define patterns consisting of 30-50 μm squares (for attachment of cell bodies) and 2-3 μm wide lines (for guided axon and dendrite growth) on chips containing fully fabricated NW FETs; the patterns were registered with respect to NW devices with ca. 1 μm accuracy. In brief, completed device chips were modified in a 1% (v/v) dichloromethane solution with (heptadecafluoro)-1,1,2,2-tetrahydrodecyldimethyl-chlorosilane (Gelest, Inc.) for 1 h, rinsed with dichloromethane and cured at 110 ^oC for 10 min. Following photolithography patterning using a positive photoresist (Shipley S1805), the fluorosilane in the exposed areas was removed by oxygen plasma (50 W for 5 minutes) and the chips were then soaked in an aqueous polylysine solution overnight (0.2-0.5 mg/ml, MW 70,000-150,000). The remaining photoresist was removed in a 30 minute acetone wash and the entire chip was sterilized by ethanol washes and a standard autoclave cycle.

Stage preparation. Fully patterned chips were mounted on a temperature-controlled microscopy platform and clamped beneath a plastic perfusion chamber. Pads without Si_3N_4 passivation extended beyond the perfusion chamber (i.e., were not in contact with the buffer solution during neuron incubation or measurement) and were wire-bonded to a set of pin sockets affixed to either side of the platform. The mounted and wired chips were sterilized (1 autoclave cycle and 1h UV-light), and then preincubated at 37 ^oC in 5% CO_2 before cell deposition.

Cell culturing. Day 18-19 embryonic primary cortical cells (or primary hippocampal cells) from Sprague/Dawley or Fischer 344 rat brain (99.9% glia-free, GTS Inc.) were suspended in culture medium (neurobasal serum-free medium containing 0.5 mM glutamine, B27 supplement and streptomycin antibiotic) and further diluted with neurobasal/glutamine/B27/streptomycin to the desired plating density. The cell suspension was transferred to sterilized and preincubated chip surfaces and incubated for 20-120 minutes at 37°C in a 5% CO_2 incubator depending on the desired cell density.

Excess cells were removed (except for a wetting layer on the chip surface) and fresh, pre-warmed medium was added. Neuron–chips were incubated at 37°C with 5% CO_2 for periods of 4-8 days.

Electrophysiology. Intracellular stimulation/recording experiments were carried out in standard manner *(6)* using glass microelectrodes back-filled with 3 M potassium chloride, and contacted with a Ag/AgCl wire (resistance 25-70 MΩ); the electrodes were mounted on motorized 3-axis micromanipulators (DC-3K, Märzhäuser Wetzlar GmbH & Co.), and controlled using standard amplifier-bridge electronics (IE-210, Warner Instrument Corp.) under computer control. All measurements were carried out at 37 °C with the chip surface submerged in an electrophysiology bath solution containing 145 mM NaCl, 3 mM KCl, 3 mM $CaCl_2$, 1 mM $MgCl_2$, 10 mM glucose and 10 mM HEPES, pH 7.25. Rest membrane potentials were estimated after entering in a whole cell configuration, and action potentials were typically elicited by brief (0.3-0.5 ms) or long (500 ms) depolarizing currents of 0.3-0.9 nA. In some experiments, tetrodotoxin (0.5-1 μM, Sigma) was introduced at specific locations using a pico-injector (PLI-100 Plus Pico-Injector , Medical Systems Corp.) or globally through bath application. All microelectrode and injection steps were made under direct optical observation, and data were recorded and processed using LabScribe.

NW-device measurements. All studies were carried out at 37 °C with the chip surface submerged in an electrophysiology bath solution (see above). The NW FET conductance was measured in AC mode (1-50 kHz; 30 mV peak-to-peak) with the DC bias set to 0V; the signal was amplified with a variable gain preamplifier (1211 current preamplifier , DL Instruments Inc.) and detected using a lock-in amplifier (DSP dual phase lock-in, Stanford Research Systems). The output data was recorded using an A/D converter at 10 or 100 kSa/s. NW-based stimulation was carried out by applying biphasic square wave pulses (amplitude 0-1 V) while inhibition/hyperpolarization was achieved by applying potential steps (amplitude 0 - 0.9 V). In both cases, the signal was applied to source and drain electrodes simultaneously.

The yield of working nanowire-neurite devices determined in large arrays (Fig. 4) is on the order of 85%. Two factors contribute to the failure of devices or <100% yield. First, during initial array fabrication ~10% of devices are not fully connected to source/drain electrodes as determined by electrical transport measurements. Second, ~5% of devices fail during cell-culture; we believe this failure is due to imperfections in the Si_3N_4 passivation layer, which exposes the metal contacts to the culture media. It should be possible to improve the yield in the future by modifying the device fabrication steps to address these points.

Estimation of NW conductance change. An electrical schematic of the NW-axon junction is shown if Fig. S10. The conductance change of the gated portion of the NW, $\Delta G_{g\text{-}Si}$, during signal propagation was estimated in the diffusive limit by $\Delta G_{g\text{-}Si} = -C_g \Delta V_g \mu / L$, where C_g is the capacitance per unit length between the NW and the electrolyte, ΔV_g is the electrochemical potential change associated with the signal spike, and μ is the NW hole mobility, 400cm^2/V-s *(7)*. There are three components to C_g due to

the (i) double layer, C_1, (ii) poly-lysine/silicon oxide layers on the NW, C_2, and (iii) quantum capacitance, C_Q. The total capacitance, $C_g = 1/(1/C_1+1/C_2+1/C_Q)$, is determined primarily by C_2 and has value of ca. 2.8×10^{-10} F/m. For typical NW/axon device parameters (contact resistance = 200 kΩ; channel length = 2.6 – 3 μm; axon diameter = 0.6-1 μm) we estimate that the total conductance change will be $\Delta G_{g\text{-}Si}$ = 13-47 μS.

Immunohistochemistry. Axons and dendrites were identified following experiments by selective antibodies using monoclonal rabbit axon-specific Tau protein antibody (1:1000 dilution, Chemicon Inc.; rabbit anti-synapsin I antibody was also used for axon labeling) and monoclonal mouse antibody MAP-2 (1:500 dilution, Chemicon Inc.), respectively (*8,9*). Neurons were fixed with 4% formaldehyde in PBS for 40 min at 4 ^{o}C, permeabilized with 0.25% Triton X-100 for 5 min and rinsed three times for 5 min with PBS. After treating with preblock-buffer (0.05% Triton-X, 5% fetal bovine serum in PBS) for 2 hours at 4^{o}C, cultures were incubated with the primary antibodies overnight in the dark at 4^{o}C. In double labeling experiments, the two primary antibodies were incubated together. Fluorophore-conjugated secondary antibodies for axons (AlexaFluor-546 anti-rabbit IgG) and dendrites (Fluorescein anti-mouse IgG) were conjugated prior to imaging with a confocal microscope system (LSM 510 Meta, Zeiss). Controls without primary antibodies and single-labeled samples were also carried out to verify the interpretation of the double-label experiments. In most cases examined, we found that the first projection extending from the neuron body along a patterned polylysine-patterned line is an axon (>80% cases, during the first 2-3 days in culture).

Supplemental Online Text

Complementary p-SiNW/n-SiNW device arrays. In devices that had alternating p-type and n-type NW elements (Fig. S2A), we observe that IC stimulation of action potential spikes in the soma yielded temporally correlated, alternating conductance peaks/dips in NW elements progressively from NW1 to NW4 (Fig. S2B). These results are consistent with gating of the p- and n-type NWs by the change in membrane potential associated with the propagating action potential, and show that we can generate complementary signals in the hybrid structures.

Modulating signal propagation with focal addition of TTX. Inputs to the hybrid NW-neuron circuit elements, as in biological neuronal networks, are not limited to electrical ones but can be chemical as well. Specifically, local release of TTX at the same input NW as used for electrical input (NW3) blocks the spike propagation and results in low output at NW5 (Fig. S8). Similar results have been reported previously using microinjection and glass microelectrodes on single neurons and neuronal one-dimensional bundles *(10,11).* A potential advantage of our approach is that a substantially higher density of recording devices can be continuously monitored independent of the repositions of the microinjector or could more easily enable the use of multiple microinjectors. Alternatively, it should be possible to release and/or detect neurotransmitters, channel blockers and other chemicals selectively using chemically-derivatized NWs, thereby enhancing the modes of input/signal modulation and output in these hybrid nanoelectronic devices.

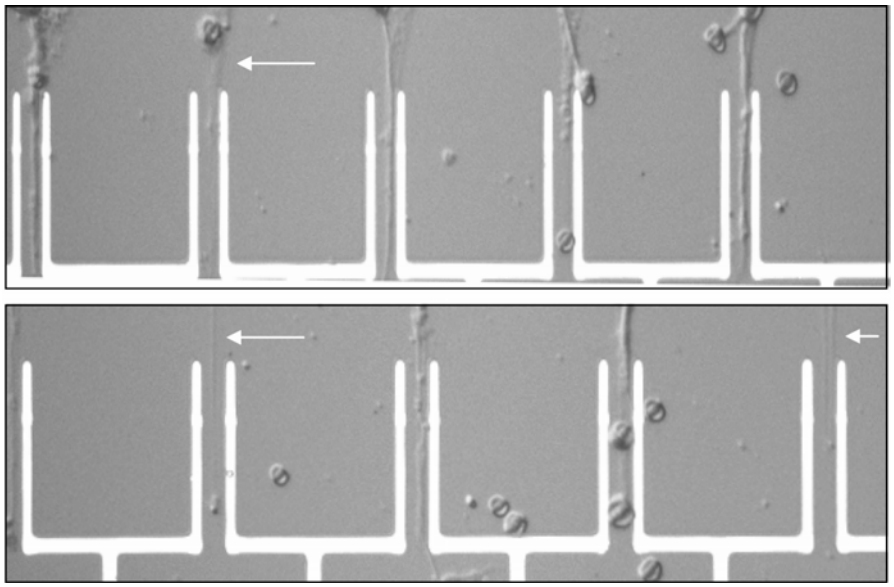

Fig. S1. Optical images of growth-directed cortex neurons on a SiNW array. The white arrows highlight the axons of individual neurons that cross NW devices.

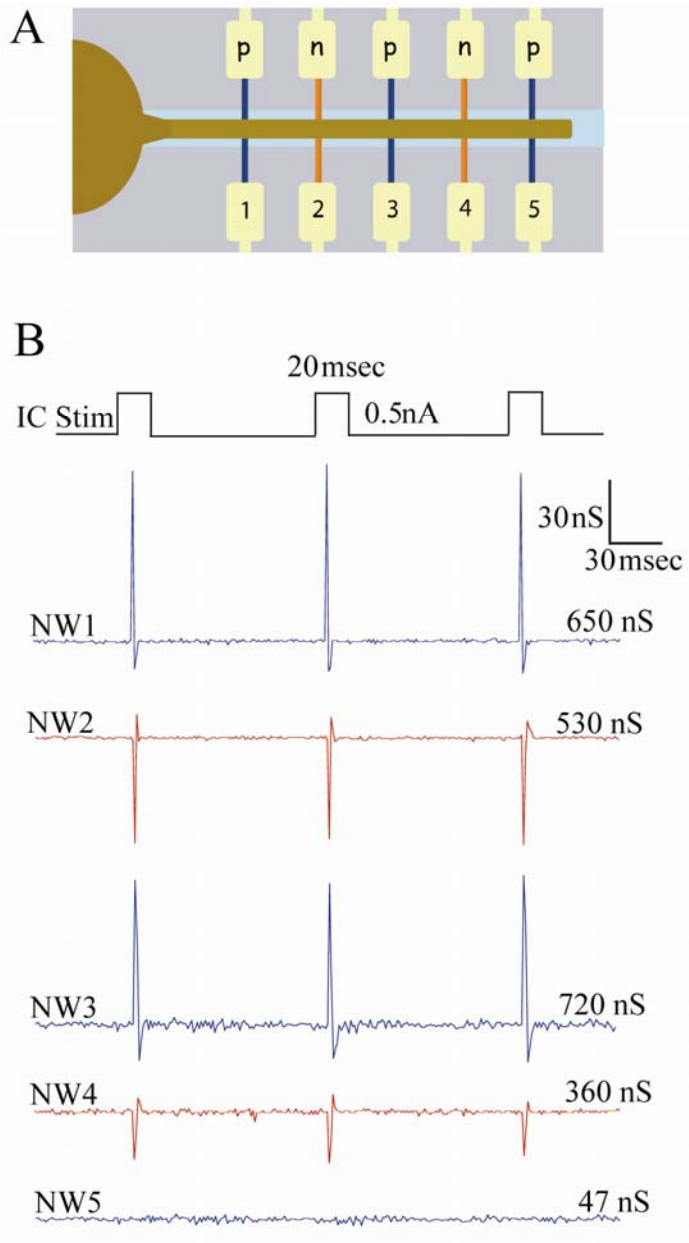

Fig. S2. Multi-NW-neuron array. (**A**) Schematic of an aligned axon crossing an alternating array of five p- and n- type NW devices. The spacing between devices is 10 μm. (**B**) Traces of intracellular current stimulation (black; 20 msec pulses of 0.5 nA amplitude) and resulting signals measured by the p-type (blue) and n-type (red) devices depicted in the preceding schematic.

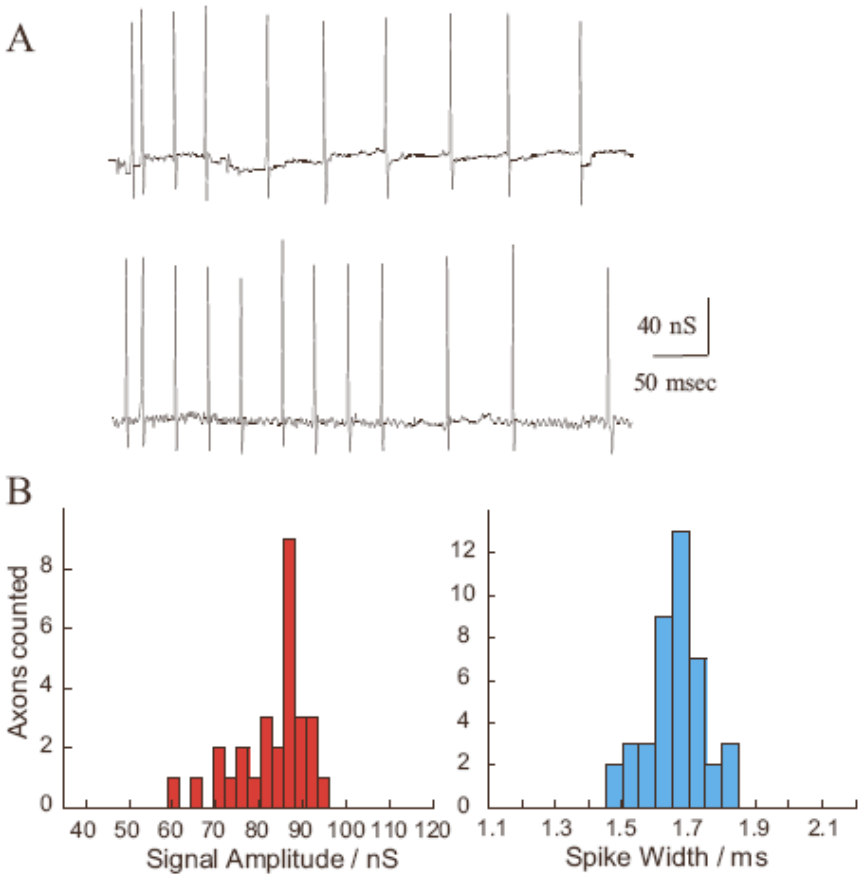

Fig. S3. NW/axon devices and controls. (**A**) NW detected action potentials for higher current intracellular stimuli of 0.3 nA (top) and 0.6 nA (bottom). The measurements were made on the same device/cell as in Fig. 1C. (**B**) Histograms of the spike amplitude (left) and width (right) measured from axons of aligned cortical neurons using p-type silicon NW devices.

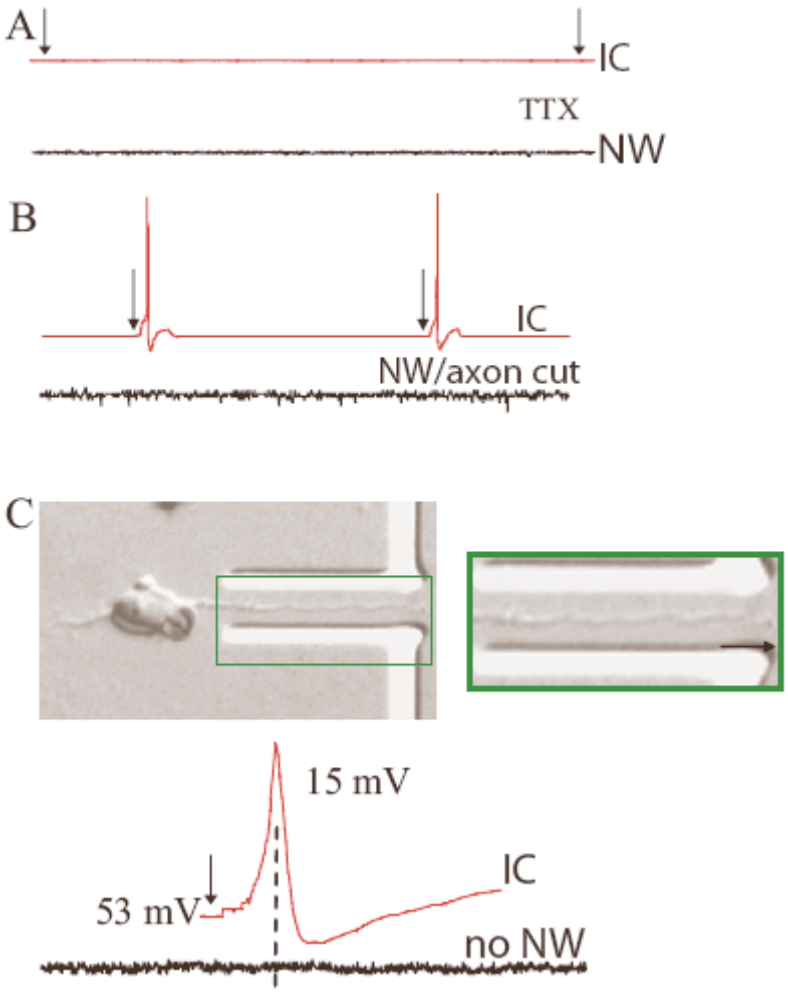

Fig. S4. (**A**) Intracellular- (red) and extracellular- (black) NW electrical responses recorded for the same system as in Fig. 1C after bath addition of 0.5 μM TTX. Small black arrows indicate start/end of intracellular stimulation pulse (0.3 nA). (**B**) Intracellular (red) and NW (black) electrical responses recorded for the same system as Fig. 1C, after severing the axon in contact with NW by using a micropipette. (**C**) (left) Optical image of a cortical neuron grown on a patterned substrate, and (right) higher resolution image of the axon passing between microfabricated electrodes without a NW element. (bottom) Intracellular (red) and microfabricated electrode (black) electrical responses.

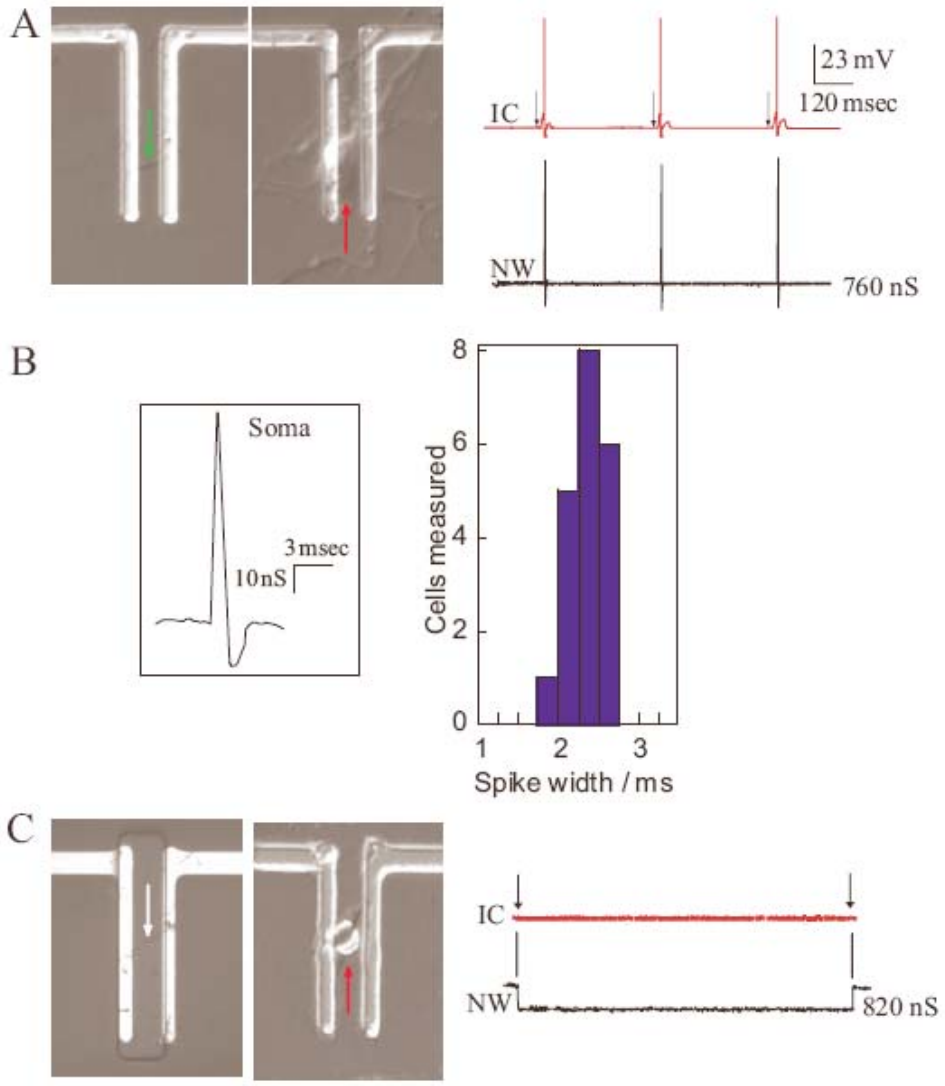

Fig. S5. NW detection of cell body signals. (**A**) (left) Silicon NW device before (left) and after (right) deposition and growth of a cortical neuron with the cell body over the NW device; the green and red arrows highlight the positions of the NW and cell body, respectively. (right) Intracellular (red) and NW (black) electrical responses of the neuron after intracellular current injection (black arrows; 15 msec, 0.6 nA pulse). (**B**) (left) Representative electrical signals detected by NW devices for individual soma-NW connections. (right) Histogram of the signal width recorded for soma/NW interfaces. (**C**) (left) Optical images of a NW device before and after the deposition of a neuron that had died. (right) Intracellular (red) and extracellular-NW (black) electrical responses recorded after intracellular stimulation of this neuron.

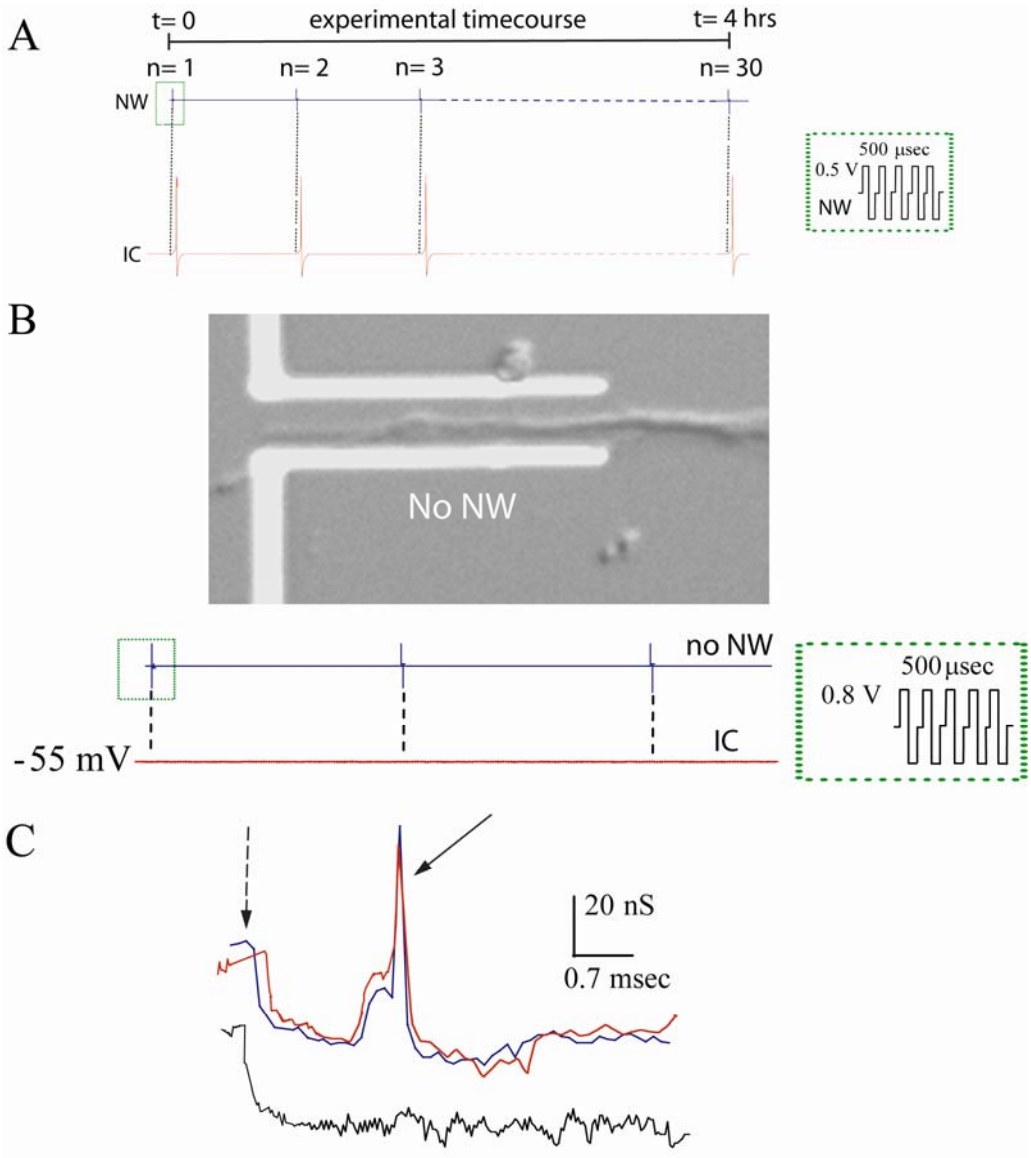

Fig. S6. NW stimulation of neurons. (**A**) Multiple stimulation experiment showing that no degredation occurs over the course of 4 hours of measurement and 30 distinct stimulation events. **(B)** (top) Optical image of the axon from a cortical neuron passing between microfabricated electrodes without a NW. Neuron growth was directed using a polylysine pattern similar to Fig. 1A. (bottom) Electrical output (stimulation curve) from the microfabricated electrodes (blue) and corresponding intracellular signal (red) following stimulation pulse sequence applied to the electrodes. The specific pulse sequence is shown in the dashed green rectangle. (**C**) NW recorded electrical responses after axonal stimulation using the same NW for stimulation (red and blue curves). Trains of five rectangular biphasic-type stimuli (train width 500 µsec; 0.5 V amplitude) are applied to the recording NW. The black curve corresponds to the NW-recorded electrical response after application of a stimuli train of five rectangular pulses of lower amplitude, 0.3 V, and equal duration as before. Solid arrow corresponds to the neuronal signal and dashed arrow corresponds to the coupling of stimulation pulse to the device output.

Input NWs (V)				Output NW (nS)
1	2	3	4	5
1 (0.9)	0	0	0	0 (750)
0	1	0	0	0
0	0	1	0	0
0	0	0	1	0
0	0	0	0	1 (825)
1	1	1	1	0

Fig. S7. Multi-NW-neurite hybrid structures. (top) Optical image of a cortex neuron with its axon aligned on an array of five p-type NW devices and (bottom) table showing input and output characteristics. NWs 1-4 act as inputs that either inhibit completely the propagation of a signal down the axon by hyperpolarizing the membrane ('1') or allow it to pass ('0'). The output, measured by NW 5, represents the presence ("1") or lack ("0") of signals that were elicited intracellularly by a micropipette electrode. The table expands upon the single point result shown in Fig. 4C for NW3. The input/output table corresponds to expected truth table for a NOR logic gate.

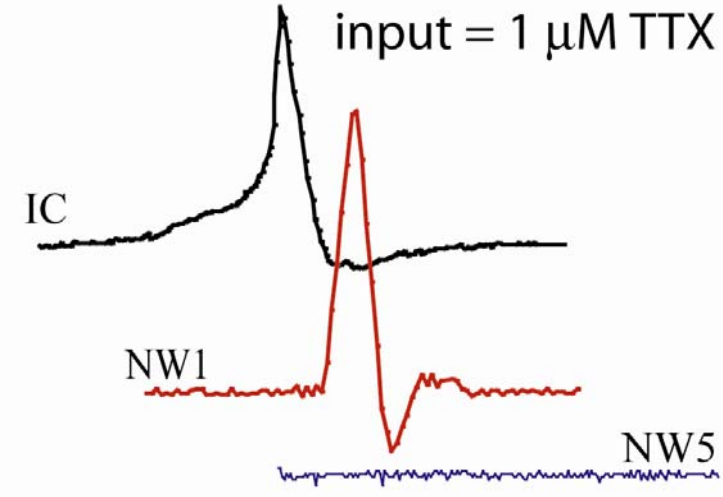

Fig. S8. Chemical modulation of signal propagation. IC and NW output signals recorded after focal application of 0.5 μM TTX to the axon section between NW3-NW4. The NW signals were recorded before (NW1) and after (NW5) the injection point of the TTX.

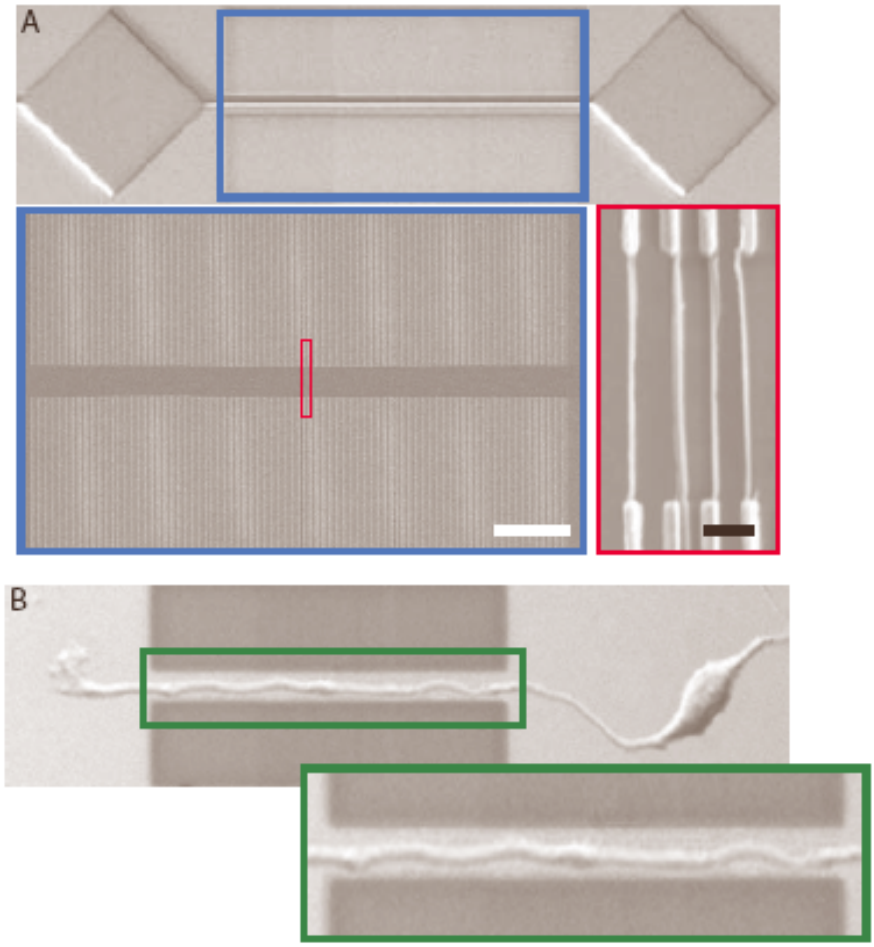

Fig. S9. High-density, multi-NW/axon hybrid structures. (**A**) (top) Optical image of a high-density device array, which is located within the open blue rectangle, with a polylysine pattern consisting of two diamonds connected by a horizontal linear stripe that runs across the center of the array. The linear array consists of 150-devices with a 400 nm device pitch. The blue rectangle is 127μm X 35 μm. (bottom left) Low magnification SEM image of the 150-device linear array; the scale bar is 8μm. (bottom right) High resolution SEM image showing 4 sequential NW devices; scale bar is 400 nm. The image was recorded from the region in the low-resolution image indicated by the open red rectangle. (**B**) Optical images recorded at increasing magnifications (top to bottom) of a rat cortical neuron with its axon aligned on a 150-device NW linear array and the soma aligned along the lower right edge of a diamond. The open green rectangle is 52 μm X 15 μm.

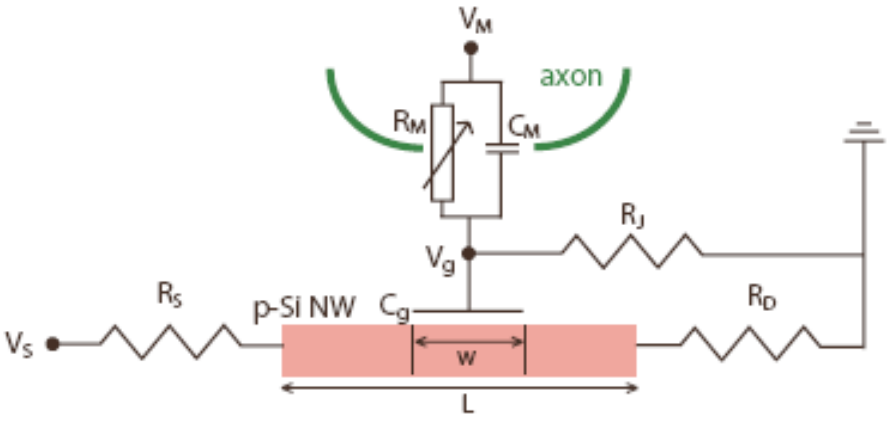

Fig. S10. Electrical model of a NW-axon junction. Schematic illustrates relevant parameters for NW FET and axon, where V_s, R_S, R_D, L, w, C_g, V_g, R_J, R_M, V_M, and C_M are the source voltage, source contact resistance, drain contact resistance, channel length, gate length, gate capacitance, gate voltage, junction resistance, axon membrane resistance, membrane potential, and membrane capacitance, respectively. The model is used for specific calculation in Methods section.

References

1. Y. Huang, C. M. Lieber, *Pure Appl. Chem.* **76**, 2051 (2004).

2. Y. Cui, Z. Zhong, D. Wang, W. U. Wang, C. M. Lieber, *Nano Lett.* **3**, 149 (2003).

3. G. F. Zheng, W. Lu, S. Jin, C. M. Lieber, *Adv. Mater***. 16**, 1890 (2004).

4. Y. Huang, X. Duan, Q. Wei, C.M. Lieber, *Science* **291**, 630 (2001).

5. S. Jin *et al., Nano Lett.* **4**, 915 (2004).

6. U. Windhorst, H. Johansson, in *Modern techniques in neuroscience research: Electrical Activity of Individual Neurons in Situ: Extra- and Intracellular* (Springer, Berlin, New York, 1999).

7. Z. Zhong, Y. Fang, W. Lu, C. M. Lieber, *Nano Lett.* **5**, 1143 (2005).

8. E. T. Kavalali, J. Klingauf, R. W. Tsien, *P. Natl. Acad. Sci. USA* **96**, 12893 (1999).

9. W. Haubensak, F. Narzm, R. Heumann, V. Leßmann, *J. Cell Sci*. **111**, 1483 (1998).

10. C. M. Colbert, D. Johnston, *J. Neurosci.* **16**, 6676 (1996).

11. O. Feinerman, M. Segal, E. Moses, *J. Neurophysiol.* **94**, 3406 (2005).